

Novel antitumor adamantane–azole gold(I) complexes as potential inhibitors of thioredoxin reductase

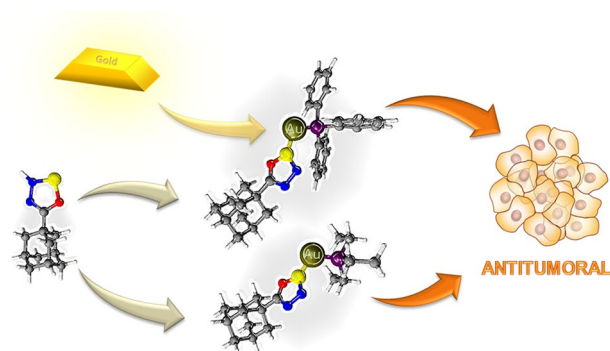
Adriana Garcia¹ · Rafael Carvalhaes Machado¹ · Richard Michael Grazul¹ · Miriam Teresa Paz Lopes² · Charlane Cimini Corrêa¹ · Hélio F. Dos Santos¹ · Mauro Vieira de Almeida¹ · Heveline Silva¹

Received: 8 July 2015 / Accepted: 9 January 2016
© SBIC 2016

Abstract Gold complexes that could act as antitumor agents have attracted great attention. Heterocyclic compounds and their metal complexes display a broad spectrum of pharmacological properties. The present study reports the preparation and characterization of four novel gold(I) complexes containing tertiary phosphine and new ligands 5-adamantyl-1,3-thiazolidine-2-thione, 3-methyladamantane-1,3,4-oxadiazole-2-thione. Spectroscopic data suggest that gold is coordinated to the exocyclic sulfur atom in all cases, as confirmed by X-ray crystallographic data obtained for complex (1) and supported by quantum–mechanical calculations. The cytotoxicity of the compounds has been evaluated in comparison to cisplatin and auranofin in three different tumor cell lines, colon cancer (CT26WT), metastatic skin melanoma (B16F10), mammary adenocarcinoma (4T1) and kidney normal cell (BHK-21). The gold complexes were more active than their respective free ligands and able to inhibit the thioredoxin reductase (TrxR) enzyme, even in the presence of albumin. Molecular modeling studies were carried out to understand the interaction between the compounds and the TrxR enzyme, considered as a potential target for new compounds in cancer treatment. The docking results show that the adamantane ring is

essential to stabilize the ligand–enzyme complex prior the formation of covalent bond with gold center.

Graphical abstract The structure of the new gold compounds was established on the basis of spectroscopic data, DFT calculations and X-ray diffraction. TrxR inhibition was evaluated and the results correlated with the assays in tumor cells, suggesting the TrxR as possible target for these compounds.



Keywords Thiazolidine · Oxadiazol · Phosphine · Thioredoxin reductase · Crystallography · Molecular docking · DFT calculations

Abbreviations

DFT	Density functional theory
DMSO	Dimethylsulfoxide
DTNB	Dithiobisnitrobenzoic acid
MTT	(3-(4,5-dimethylthiazol-2-yl)-2,5-diphenyltetrazolium bromide
NADPH	Nicotinamide adenine dinucleotide phosphate
NMR	Nuclear magnetic resonance
PEt ₃	Triethylphosphine
PPh ₃	Triphenylphosphine
RPMI	Roswell Park Memorial Institute Medium

Electronic supplementary material The online version of this article (doi:10.1007/s00775-016-1338-y) contains supplementary material, which is available to authorized users.

✉ Heveline Silva
hevelinequi@gmail.com

¹ Departamento de Química, ICE, Universidade Federal de Juiz de Fora, Juiz De Fora, MG 36036-900, Brazil

² Departamento de Farmacologia, ICB, Universidade Federal de Minas Gerais, Belo Horizonte, MG 31270-901, Brazil

TMS	Tetramethylsilane
TNB	5-thionitrobenzol
TrxR	Thioredoxin reductase

Introduction

Gold has been used in medicine since ancient times [1], but only after 1935, when Forestier described the anti-arthritic properties of gold(I) compounds [2], the scientific community started the investigation of their beneficial and toxic effects. Compounds like myochrysin (sodium gold(I)thiomalate), solganal (gold(I)thioglucose) and auranofin (triethylphosphine-(2,3,4,6-tetra-*O*-acetyl- β -1-D-thiopyranosato-S)gold(I)) are still used in the treatment of rheumatoid arthritis [3].

Auranofin has been tested as antitumor drug in several cell lines, showing potent cytotoxic activity, especially for leukemia [4, 5]. The malfunction of biochemical pathways is related to the cellular pathophysiology of rheumatoid arthritis, which is also important in cancer development [6]. The possibility of gold complexes to act as antitumor agents has attracted great attention. Many of the tested compounds were effective to inhibit the growth of tumor cells and have potential for treating cisplatin-resistant tumors [7–9]. Nonetheless, the mechanism of action for gold complexes is still unclear; many studies suggested that the biological effect could be mediated by an anti-mitochondrial mechanism, anti-inflammatory pathways decreasing TNF- α (tumor necrosis factor) or even increasing production of reactive oxygen species (ROS) inducing apoptosis [3, 5, 10]. The enzyme thioredoxin reductase (TrxR) is over expressed in many cancer cells indicating its involvement in proliferation of tumor tissues [11–13]. TrxR plays an important role in the regulation of intracellular redox balance [5, 11]. Phosphine gold(I) complexes, such as auranofin, also interact with glutathione, serum proteins as albumin, cellular proteins and other small molecular weight thiols-containing biomolecules [3, 14]. Auranofin has also been shown to inhibit ubiquitin–proteasome system that mediates protein degradation through a cascade process, an important target for cancer and other diseases [15].

Several gold-based compounds have been reviewed over the last decades as potential candidates as anticancer agents [16, 17]. Using molecules that exhibit biological activity as ligands could enhance the activity of the complex by a synergistic mechanism or via multiple mechanism of action [18]. Compounds derived from adamantane are present in commercial drugs such as amantadine and memantine which are used to treat Parkinson's and Alzheimer's diseases, respectively. These molecules also present other biological actions, including potential anticancer activity

[19–22]. On the other hand, heterocyclic ligands such as 1,3-thiazolidines and 1,3,4-oxadiazolines belong to classes of compounds that exhibit a broad spectrum of pharmacologic activity. There are reports of antimicrobial, antifungal and antihelminthic activity. Furthermore, they are present in many natural products and pharmaceutical drugs such as nesapidil, penicillin and pioglitazone [23–27]. In a previous work we reported synthesis, characterization and biological activity for four gold complexes containing thiazolidinic and oxadiazolic moieties demonstrating cytotoxic activity and high selectivity when investigated against tumoral and non-tumoral cells [28]. In that study the structure–activity relationship was not clear and the complexes were not tested as TrxR inhibitors; therefore the action mechanism could not be completely investigated. Other phosphane gold complexes with thiazole groups were investigated with respect to their interactions with the TrxR enzyme and cytotoxicity revealing important biological effects [29].

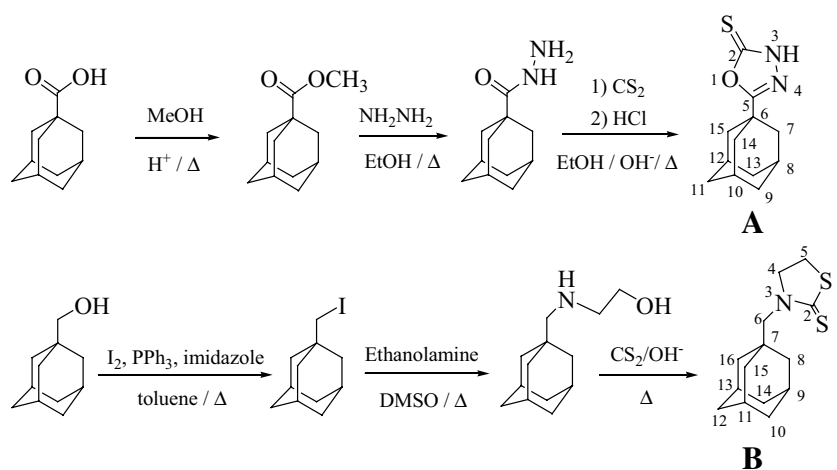
The hydrophilic and lipophilic balance of the aryl ligand is another important property which should be considered since increasing the lipophilicity enhances the rate of cellular uptake and the cytotoxic activity [30]. Some previous structure–activity relationship studies of gold(I) compounds and auranofin have shown that complexes coordinated to tertiary phosphines are more active than similar compounds with no phosphine substituents. The introduction of a tertiary phosphine also increases the lipophilicity which, in turn, increases the permeability through the cell membrane [31].

In the present study, we describe the synthesis, characterization, including, single-crystal X-ray diffraction data, cytotoxic activity against tumor cell lines and the inhibition of TrxR for four new gold(I) complexes with ligands derived from adamantane containing the heterocyclic 1,3-thiazolidines or 1,3,4-oxadiazolines and tertiary phosphine (PEt₃ or PPh₃). Molecular modeling was conducted to assist experimental data analysis, including structural prediction, vibrational and NMR spectroscopies and the reactivity of the complexes against a selenocystein (Sec) residue. Docking studies were also performed for the main derivatives considering the TrxR as the biological target.

Experimental

Materials and methods

All reagents and solvents were used without further purification. Infrared (IR) spectra were recorded on a BRUKER ALPHA FT-IR Spectrometer, in the region of 4000–400 cm⁻¹ as a KBr pellet, with a spectral resolution of 4 cm⁻¹ and an average of 64 scans. Raman spectra were obtained using a Bruker RFS 100 FT-Raman instrument

Scheme 1 Synthesis of ligands **a** and **b**

equipped with a germanium detector refrigerated by liquid nitrogen, with excitation at 1064 nm from a Nd:YAG laser, in the range between 4000 and 50 cm^{-1} and a spectral resolution of 4 cm^{-1} , with an average of 500 scans. ^1H NMR (300 MHz) and ^{13}C NMR (75 MHz) spectra were recorded in CDCl_3 solutions on a BRUKER AVANCE DRX/300 spectrometer. The chemical shifts were expressed in the δ scale (ppm) relative to TMS internal standard. ^{31}P NMR (202 MHz) spectra were recorded in acetone solutions on a Avancer III HD BRUKER 500 MHz. The chemical shifts were expressed in the δ scale (ppm) relative to H_3PO_4 external standard. The TG/DTA curves were obtained with a SHIMADZU DTG-60 Simultaneous DTA-TG apparatus under a dynamic nitrogen atmosphere (heating rate 10 $^\circ\text{C min}^{-1}$ and temperature range from room temperature to 500 $^\circ\text{C}$). Mass spectra were obtained on an AXIMA MALDI-TOF-TOF Shimadzu Biotech instrument. A nitrogen laser ($\lambda_{\text{max}} = 337 \text{ nm}$) was employed for excitation in an α cyano matrix. 200 scans were accumulated with 20 repetitions each. Elemental analyses were performed at Central Analítica, USP-Brazil. Diffraction data for single crystals were collected using an Oxford GEMINI A Ultra diffractometer with Mo $\text{K}\alpha$ ($\lambda = 0.71073 \text{ \AA}$) and temperature of 298 K. Data collection, reduction and cell refinement were carried out by CRYCALISRED, Oxford diffraction Ltd., Version 1.171.32.38 software [32]. The structures were solved and refined using SHELXS-97 and SHELXL-97, respectively [33]. An empirical isotropic extinction parameter x was refined, according to the method described by Larson [34]. A Multiscan absorption correction was applied [35]. Anisotropic displacement parameters were assigned to all non-hydrogen atoms. The O- and N-bound H atoms were initially located in a difference Fourier map, then added in idealized positions and further refined according to the riding model, with N–H = 0.86 \AA , and with $\text{Uiso}(\text{H}) = 1.5\text{Ueq}(\text{O})$ or $1.2\text{Ueq}(\text{N})$. C-bound H atoms were included in the riding-model approximation, with C–H = 0.95 \AA and

$\text{Uiso}(\text{H}) = 1.2\text{Ueq}(\text{C})$. The structures were drawn by ORTEP-3 for Windows [36] and MERCURY softwares [37]. Ultraviolet (UV) spectra were recorded on a SHIMADZU UV-1800 spectrophotometer in quartz cuvettes.

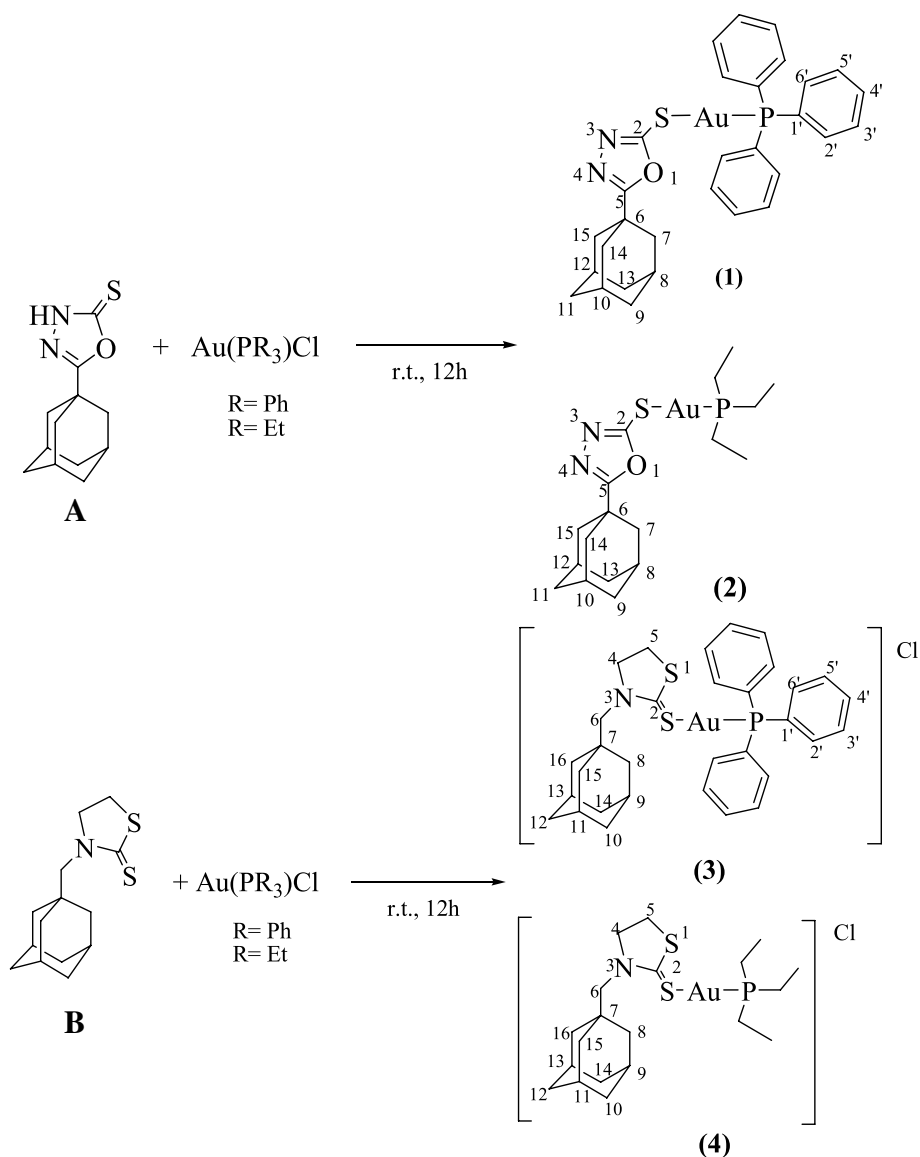
Synthesis of ligands (Scheme 1)

Ligand (**A**) was previously reported and prepared according to the method described in the literature [23, 27, 38]. Adamantane-1-carboxylic acid was esterified with methanol under acidic conditions for 24 h at 90 $^\circ\text{C}$. The ester was reacted with hydrazine (hydrate 64 %) in ethanol at 80 $^\circ\text{C}$ for 5 days and the hydrazide thus formed was treated with carbon disulfide under basic conditions in ethanol, followed by subsequent acidification with HCl (6 M) to pH 6 at 80 $^\circ\text{C}$ for 5 days. The final product (**A**) was purified by recrystallization and the obtained crystals were analyzed by single crystal X-ray diffraction.

(**A**): yellow solid. TG/DTA: 190–191 $^\circ\text{C}$ (mp). IR ν_{max} KBr (cm^{-1}): 3122, 3092, 2914, 2850, 1605, 1504, 1452, 1181, 752. ^1H NMR [300 MHz, CDCl_3 , δ (ppm)]: 1.7–2.0 (*m*, 15H, H-adamantyl); 11.7 (*s*, 1H, N–H). ^{13}C NMR [75 MHz, CDCl_3 , δ (ppm)]: 26.7; 28.5; 36.2; 40.9 (C-adamantyl); 170.6 (C5); 178.5 (C2).

Ligand (**B**) was prepared from 1-adamantane methanol as described in the literature [39]. The alcohol was treated initially with triphenylphosphine, imidazole and iodine in toluene for 24 h at 90 $^\circ\text{C}$. The replacement of the iodine in the 1-adamantane methyl iodide was effected by reaction with ethanolamine in DMSO for 24 h at 100 $^\circ\text{C}$. The product was purified by column chromatography. The final step consisted of the cyclization of the amino alcohol with carbon disulfide under basic conditions for 12 h at 80 $^\circ\text{C}$. The final product (**B**) was purified by recrystallization and the obtained crystals were analyzed by single crystal X-ray diffraction.

(**B**): white solid. TG/DTA: 168–169 $^\circ\text{C}$ (mp). IR ν_{max} KBr (cm^{-1}): 2905, 2845, 1481, 1413, 1296, 1229. ^1H

Scheme 2 Synthesis of complexes (1), (2), (3) and (4)

NMR [300 MHz, CDCl₃, δ (ppm), J (Hz)]: 1.6–2.0 (*m*, 15H, H-adamantyl); 3.2 (*t*, 2H, H5, $J_{5,4} = 7.4$); 3.4 (*s*, 2H, H6); 4.1 (*t*, 2H, H4, $J_{5,4} = 7.4$). ¹³C NMR [75 MHz, CDCl₃, δ (ppm)]: 27.4; 28.2; 36.7; 41.3 (C-adamantyl); 36.6 (C5) 59.9 (C4) 61.0 (C6); 198.5 (C2).

Synthesis of the gold(I) complexes (Scheme 2)

Au(PPh₃)Cl was synthesized from K[AuCl₄] according to the literature [40] and Au(PEt₃)Cl is commercially available. Complexes **(1)** and **(2)** were obtained from ligand **(A)** (0.4 mmol) dissolved in dichloromethane (5 mL) which was added to a solution of Au(PPh₃)Cl (0.4 mmol) or Au(PEt₃)Cl (0.4 mmol) in dichloromethane (5 mL). After stirring for 5 h at room temperature, K₂CO₃ (0.2 mmol) was added to adjust the pH. After 7 h the complete consumption of the starting materials was

evidenced by thin layer chromatography (TLC) (eluent: 9:1 dichloromethane/methanol). The product was purified by a liquid/liquid extraction with dichloromethane/water to eliminate carbonate and the solvent of the organic phase was removed under reduced pressure to give the desired compounds **(1)** and **(2)** in 88 and 92 % yields, respectively.

Complexes **(3)** and **(4)** were obtained from ligand **(B)** (0.4 mmol) dissolved in dichloromethane (5 mL) and added to a solution of Au(PPh₃)Cl (0.4 mmol) or Au(PEt₃)Cl (0.4 mmol) in dichloromethane (5 mL). After stirring for 12 h at room temperature the complete consumption of the starting materials was evidenced by thin layer chromatography (TLC) (eluent: 9:1 dichloromethane/methanol). The solvent was removed under reduced pressure to furnish the desired compounds **(3)** and **(4)** in 82 and 90 % yields, respectively.

(1): beige solid. TG/DTA: 218–219 °C (mp). IR ν_{\max} KBr (cm^{-1}): 3051, 2916, 2848, 1452, 1145, 1101, 748, 692, 540, 501. ^1H NMR [300 MHz, CDCl_3 , δ (ppm)]: 1.7–2.1 (*m*, 15H, H-adamantyl); 7.2–7.7 (*m*, 15H, Ar-PPh₃). ^{13}C NMR [75 MHz, CDCl_3 , δ (ppm), J (Hz)]: 27.7; 35.1; 36.4; 39.7 (*s*, C-adamantyl); 128.9 (*d*, 1J (C,P) = 62.4, *ipso*-C from PPh₃); 129.5 (*d*, 3J (C,P) = 12.0, *meta*-C from PPh₃); 132.2 (*d*, 4J (C,P) = 2.7, *para*-C from PPh₃); 134.4 (*d*, 2J (C,P) = 13.8, *ortho*-C from PPh₃); 160.3 (*s*, C5); 176.2 (*s*, C2). $^{31}\text{P}\{^1\text{H}\}$ NMR [202 MHz, acetone, δ (ppm)]: 25.22 (*s*).

Anal. Calc. for $[\text{C}_{30}\text{H}_{30}\text{N}_2\text{OPSAu}]$: C, 51.88; H, 4.35; N, 4.03. Found: C, 51.49; H, 4.35; N, 3.98 %.

MS (MALDI): m/z Calc. for $[\text{C}_{30}\text{H}_{30}\text{N}_2\text{OPSAu}]$ $[\text{M} + \text{H}]^+$ Calc. (695.6) found 695.5.

(2): beige solid. TG/DTA: 144–145 °C (mp). IR ν_{\max} KBr (cm^{-1}): 2964, 2904, 2848, 1454, 1145, 769. ^1H NMR [300 MHz, CDCl_3 , δ (ppm)]: 1.2–1.3 (*m*, 9H, CH₃); 1.6–2.0 (*m*, 21H, H-adamantyl, P(CH₂-CH₃)₃). ^{13}C NMR [75 MHz, CDCl_3 , δ (ppm), J (Hz)]: 9.2 (*s*, P(CH₂-CH₃)₃); 18.1 (*d*, J (C-P) = 35, from PEt₃); 27.5; 36.0; 38.8; 39.6 (*s*, C-adamantyl); 168.5 (*s*, C5); 174.6 (*s*, C2). $^{31}\text{P}\{^1\text{H}\}$ NMR [202 MHz, acetone, δ (ppm)]: 38.90 (*s*).

Anal. Calc. for $[\text{C}_{18}\text{H}_{30}\text{N}_2\text{OPSAu}]$: C, 39.28; H, 5.49; N, 5.09. Found: C, 39.29; H, 5.42; N, 4.91 %.

MS (MALDI): m/z Calc. for $[\text{C}_{18}\text{H}_{30}\text{N}_2\text{OPSAu}]$ $[\text{M} + \text{H}]^+$ Calc. (551.4) found 551.3.

(3): yellow solid. TG/DTA: 162–163 °C (mp). IR ν_{\max} KBr (cm^{-1}): 3058, 2906, 2844, 1481, 1413, 1296, 1230, 1149, 1101, 748, 692, 545, 501. Raman ν_{\max} (cm^{-1}): 329 (Au-S). ^1H NMR [300 MHz, CDCl_3 , δ (ppm), J (Hz)]: 1.6–2.0 (*m*, 15H, H-adamantyl); 3.2 (*t*, 2H, H5, $J_{5,4} = 7.4$); 3.4 (*s*, 2H, H6); 4.1 (*t*, 2H, H4, $J_{4,5} = 7.4$); 7.5–7.6 (*m*, 15H, Ar-PPh₃). ^{13}C NMR [75 MHz, CDCl_3 , δ (ppm), J (Hz)]: 27.8; 28.4; 36.9; 41.5 (*s*, C-adamantyl); 37.0 (*s*, C5); 60.4 (*s*, C4); 61.4 (*s*, C6); 128.9 (*d*, 1J (C,P) = 62.5, *ipso*-C from PPh₃); 129.4 (*d*, 3J (C,P) = 11.9, *meta*-C from PPh₃); 132.2 (*d*, 4J (C,P) = 2.3, *para*-C from PPh₃); 134.4 (*d*, 2J (C,P) = 13.7, *ortho*-C from PPh₃); 198.9 (*s*, C2). $^{31}\text{P}\{^1\text{H}\}$ NMR [202 MHz, acetone, δ (ppm)]: 33.19 (*s*).

Anal. Calc. for $[\text{C}_{32}\text{H}_{36}\text{NPS}_2\text{Au}]\text{Cl}$: C, 50.43; H, 4.76; N, 1.84. Found: C, 50.71; H, 4.85; N, 1.91 %. MS (MALDI): m/z Calc. for $[\text{C}_{32}\text{H}_{36}\text{NPS}_2\text{Au}]^+ [\text{M}]^+$ Calc. (726.7) found 726.5.

(4): yellow solid. TG/DTA: 112–113 °C (mp). IR ν_{\max} KBr (cm^{-1}): 2964, 2906, 2844, 1483, 1415, 1296, 1230, 1149, 771. Raman ν_{\max} (cm^{-1}): 314 (Au-S). ^1H NMR [300 MHz, CDCl_3 , δ (ppm), J (Hz)]: 1.1–1.2 (*m*, 9H, CH₃); 1.6–1.9 (*m*, 21H, H-adamantyl, P(CH₂-CH₃)₃); 3.2 (*t*, 2H, H5, $J_{5,4} = 7.4$); 3.4 (*s*, 2H, H6); 4.1 (*t*, 2H, H4, $J_{4,5} = 7.4$). ^{13}C NMR [75 MHz, CDCl_3 , δ (ppm), J (Hz)]: 8.9 (*s*, P(CH₂-CH₃)₃); 18.2 (*d*, J (C-P) = 37 Hz, from PEt₃); 27.6; 28.3; 36.7; 41.4 (*s*, C-adamantyl); 36.8 (*s*, C5); 60.1 (*s*,

C4); 61.2 (*s*, C6); 198.5 (*s*, C2). $^{31}\text{P}\{^1\text{H}\}$ NMR [202 MHz, acetone, δ (ppm)]: 33.43 (*s*).

Anal. Calc. for $[\text{C}_{20}\text{H}_{36}\text{NPS}_2\text{Au}]\text{Cl}$: C, 38.87; H, 5.87; N, 2.27. Found: C, 38.92; H, 5.47; N, 2.09 %.

MS (MALDI): m/z Calc. for $[\text{C}_{20}\text{H}_{36}\text{NPS}_2\text{Au}]^+ [\text{M}]^+$ Calc. (582.6) found 582.4.

Cytotoxicity assay

Cytotoxicity activity was investigated against the non-tumor cell BHK-21—Baby Hamster Kidney and the following tumor cell lines: CT26-WT—murine colon cancer cells, B16-F10—mouse metastatic melanoma and 4T1—mouse metastatic mammary adenocarcinoma.

Cells were harvested and seeded in RPMI 1640 culture medium, pH 7.4, supplemented with 10 % Fetal Bovine Serum (FBS) at cell densities that varied depending on the cell line, 0.5×10^3 and 2×10^3 cells/100 μL /well in a plate with 96 wells and were then incubated at 37 °C in a humidified atmosphere of 5 % CO₂ for 24 h for optimum adhesion. Stock solutions of all compounds in DMSO were serially diluted (100–0.1 μM) in cell culture medium (<1 % DMSO). After drug exposure for 72 h the cells were incubated with MTT (5 $\mu\text{g}/10 \mu\text{L}$ /well) for 4 h. MTT is metabolized by viable cells resulting in a violet complex product that, after being solubilized in 100 μL DMSO/well, can be quantified through colorimetric assay using a plate reader (absorbance at 570 nm). Cisplatin and auranofin were used as positive control against these cell lines. The raw data were normalized to cell viability of the negative control (culture medium with no compounds) as 100 %. The IC₅₀ values were calculated by four parametric nonlinear regressions using GraphPad Prism 5.0 software.

An equivalent experiment was performed using 4T1 cells and BHK-21 with some modifications [41]: 24 h after the cells were seeded, bovine serum albumin (BSA, non-toxic final concentration, 2 mg/mL) was added followed by addition of gold compounds. IC₅₀ values were obtained as described above.

Inhibition of thioredoxin reductase (TrxR) activity

Rat liver TrxR (Sigma) was used to determine TrxR inhibition by the compounds. The assay was performed according to the manufacturer's instructions (Sigma T9698) with appropriate modifications. Initially, 20 μL of compounds (final concentration 5 μM in 5 % DMSO/potassium phosphate buffer, pH 7.0) were added to 20 μL of TrxR water solution (approximately 0.10 units) and incubated for 1 h at 37 °C. After incubation, 600 μL of reaction mixture containing substrate dithiobisnitrobenzoic acid (DTNB) was added and the formation of 5-thionitrobenzyl (TNB) was monitored in SHIMADZU UV-Visible

Spectrophotometer (UV-1601PC) at 412 nm for 4 min. The reaction mixture consisted of 200 μL of 500 mM EDTA solution pH 7.5, 800 μL of DTNB solution (63 mM) in ethanol, 50 μL of nicotinamide adenine dinucleotide phosphate (NADPH) (48 mM), 100 μL of 20 mg/mL bovine serum albumina(BSA), 1 mL of 1.0 M potassium phosphate buffer and 7.85 mL of water. The absorbance was obtained from two independent experiments in triplicate. The enzymatic activity of the samples was calculated in percentage using the absorbance of the positive control (no inhibitor) as maximum activity (100 %). The blank solutions were prepared as samples described above for each compound without TrxR.

Glutathione interaction

Phosphate buffer pH 7.0 solutions containing gold complexes were prepared (DMF: 0.5 % v/v) at 500 μM . Aqueous solutions of reduced glutathione (GSH) from Sigma were used at 250 μM . The experiment was performed in a 96-well plate. Each well received 25 μL of GSH solution, 25 μL of buffer containing gold complexes or DMF as control, 25 μL of 100 mM aqueous EDTA solution pH 7.5 and incubated at 37 $^{\circ}\text{C}$ for 1 h. To each well, 200 μL of reaction mixture (1000 μL reaction mixture consisted of 620 μL potassium phosphate buffer pH 7.0, 80 μL , 100 mM EDTA solution pH 7.5, and 300 μL distilled water) was added, and the reaction was started with the addition of 25 μL of a 20 mM ethanolic solution of DTNB. The formation of 5-TNB was monitored in a microplate reader at 405 nm [13].

DFT and docking studies

Calculations were carried out at distinct levels depending on the property desired. Firstly the geometries of the ligands (**A** and **B**) and gold(I) complexes (**1–4**) were optimized in the gas phase at a density functional theory (DFT) level with hybrid three-parameter B3LYP functional [42] and 6-31+G(2d) basis sets for all atoms, except gold, which was treated with the ECP-SDD [43] augmented with one set of f polarization function ($\alpha_f = 1.13863280$) [44–46] (hereafter abbreviated as B3LYP/6-31+G(2d)/SDD(f)). Vibrational spectra were calculated and assigned in the gas phase at the very same level of theory used for obtaining the geometries. ^1H and ^{13}C NMR spectra were predicted at the B3LYP/6-31+G(2d,p)/SDD(f) level in CHCl_3 ($\epsilon = 4.711$) where the solvent was included through the IEF-PCM formalism [47] using the UFF radii to define the solute cavity. The chemical shift was referenced to TMS.

The ligand exchange reaction paths for all four complexes were calculated considering the Sec amino acid as the entering group. The Sec structure was considered in

its neutral zwitterionic form, regardless of the pK_a of the side chain. The transition state (TS) structures were first optimized and characterized as first-order saddle point on the PES through harmonic vibrational analysis (only one imaginary frequency). Then, the activation free energy (ΔG_a) and reaction free energy (ΔG_r) were obtained using infinitely separate reactants. The reaction paths were calculated in aqueous solution (IEF-PCM, $\epsilon = 78.355$) at the B3LYP/6-31+G(2d)/SDD(f) level with $T = 298.15$ K and $p = 1$ atm. The quantum mechanical calculations were carried out using Gaussian 09, Revision A.02 [48].

The docking studies were conducted using the GOLD[®] package [49–51]. The human TrxR1 crystal structure coded 2J3 N in the PDB was taken as a target [52]. This structure has the Sec-498 residue (at the end of the C-terminal arm) mutated to Cys-498, which is at the solvent exposure region in the reduced form of the enzyme and represents the main local binding site. The unit cell is composed of three dimers and only the pair C–D was considered with two FAD and two NADP⁺ molecules in addition to the ligand 2-methyl-2,4-pentanediol (MPD). The enzyme was first prepared by adding hydrogens using standard protonation states at physiological pH and removal of the NADP⁺ cofactor and MPD ligand. The docking site was chosen at the C-terminal motif defined as a spherical region of 15 Å centered on the sulfur atom of the Cys-498 residue. The GOLD[®] program uses genetic algorithm (GA) to explore the ligand–protein binding space [49–51]. Here, 100 GA runs were carried out for the free ligands (**A**) and (**B**) and the top 100 docking *poses* scored using the piecewise linear potential (PLP) scoring function. The docking for ligands on the TrxR binding site was performed without any constraint applied. For the gold complexes (**1–4**), 50 GA runs were analyzed and the corresponding *poses* scored with PLP scoring function. As the gold atom is not formally accounted for in the searching algorithms and scoring function, the distance between the sulphur atom of Cys-498 (considered the center of the enzyme binding site) and gold atom was constrained within the 1.5–3.5 Å range in the docking procedure with the spring constant (k) set to 5 (in arbitrary units). In the GOLD[®] program [49–51], if the constrained distance is found outside the specified bounds, spring energy is used to reduce the fitness score ($E = kx^2$: x is the difference between the bounds and actual distance values). The intermolecular interactions of the best *poses* were analyzed using the Discovery Studio 4.0 software [53], which was also used to produce the images.

Results and discussion

All compounds were synthesized in good yields (over 80 %) and after recrystallization, ligands and complex (**1**)

were obtained as single crystals. All compounds were characterized by NMR, infrared and Raman spectroscopies, elemental analyses, mass spectroscopy and X-ray diffraction. According to the results of TG/DTA, all complexes were found to be thermally stable up to 200 °C and endothermal decomposition was preceded by melting. The mass spectra showed pseudomolecular ions $[M+H]^+$ of compounds (1) and (2), and $[M]^+$ for compounds (3) and (4) in accordance with the structures proposed in scheme 2.

IR and Raman vibrational analysis

Ligand (A) can exist in two tautomeric forms with the thione form (NH) predominating in solution. At B3LYP/6-31+G(2d,p)/SDD(f) level, the thione form was 11.8 kcal mol⁻¹ more stable than the thiol tautomer (SH) in CHCl₃ solution. The IR spectra for complexes (1) and (2) were analyzed in comparison to the IR of the ligand (A) and complexes (3) and (4) were compared to the IR of ligand (B). The infrared spectrum of ligand (A) shows absorptions corresponding to ν_{N-H} at 3122, 3092 and 1505 cm⁻¹. The 2914 and 2850 cm⁻¹ regions show absorptions due to CH₂ and CH groups. Other absorptions that were observed are: ν_{CN}/δ_{NH} (1605 and 1181 cm⁻¹) and ν_{CS} (750 cm⁻¹). In the IR spectra of complexes (1) and (2), in addition to the absorptions observed for the ligands, we have noticed the absence of ν_{N-H} and thioamide bands [54].

Ligand (B) shows absorptions in the regions of 2905 and 2845 cm⁻¹ assigned to CH₂ and CH. The thioamide bands were observed at 1481 and 1296 cm⁻¹ resulting from vibrational coupling of N=C=S. The absorptions at 1229 cm⁻¹ were attributed to δ_{CN} [54]. In the IR spectra of complexes (3) and (4) no significant changes were observed. The IR spectra of complexes (1) and (3) show absorptions attributable to PPh₃ in the regions of 3050, 1145, 1101, 748, 692, 540, 501 cm⁻¹.

The main Raman assignments are shown in Tables S1 and S2 for the series of compounds derived from ligands (A) and (B), respectively. Experimental data for ligand (A) and complex (1) are given in Table S1. For complex (2) the experimental Raman spectrum was of low quality and could not be assigned, therefore only theoretical data are provided. The oxadiazoline vibrational modes were assigned experimentally for ligand (A) at 1606 (ν_{C5N4}), 1441 (ν_{C2N3}), 1169 (ν_{C2O1}), 1062 (ν_{N3N4}) and 1044 cm⁻¹ (ν_{C5O1}) with the former being quite sensitive to the gold(I) coordination. In complex (1), for which a Raman spectrum was obtained, the ν_{C5N4} stretching frequency was at 1566 cm⁻¹, a shift of 40 cm⁻¹ comparing to the free ligand (A). A red shift was also predicted theoretically from 1646 to 1606 cm⁻¹, with calculated frequencies overestimated as expected for the harmonic oscillator approach. The ν_{C2N3} mode also suffers some

influence from gold(I) coordination; however, it is not clear experimentally because of the coupling with the $\delta_{ip}(NNH)$ deformation in the free ligand. Similar arguments can be used for the ν_{N3N4} stretching, which is predicted to shift -51 cm⁻¹ from ligand (A) to complex (1), but could not be assigned experimentally due to the overlapping of intense phosphine vibrations at 1034 cm⁻¹. The assignment of the low frequency region is quite complex due to the strong coupling of vibrational modes and low intensity. Experimentally, the ν_{AuS} was attributed for complex (1) at 377 cm⁻¹. Theoretically two modes have contribution from ν_{AuS} stretching at 294 and 369 cm⁻¹. For complex (2), only theoretical data are provided at 295 and 370 cm⁻¹ and do not differ significantly from those calculated for complex (1).

The Raman spectra for ligand (B) exhibited several bands, most of them assigned as CH₂ vibrations (Table S2), which overlap with the most relevant vibrations from the heterocyclic ring. These main bands are at 1481 (ν_{C2N3}), 1298 (ν_{C4N3}), 1232 (ν_{C6N3}), 1061 (ν_{C2S}), 987 (ν_{C4C5}) and 700 cm⁻¹ (ν_{C5S1}) for the free ligand (B). In general, the position of these bands is not very sensitive to gold coordination, except for the one assigned to ν_{C2N3} , which is predicted to shift to the blue region by ~20 cm⁻¹, though, this was not observed experimentally. Indeed, an increase of the C2N3 bond order is expected after the gold coordination due to the electron delocalization over the N3-C2-S moiety, passing from N-C=S to N=C-S canonical form. The C2-N3 bond lengths for (B) and (4) were calculated as 1.36 and 1.33 Å, respectively. The ν_{AuS} stretching was experimentally assigned at 330 and 314 cm⁻¹ for (3) and (4), respectively. Theoretically, two vibrations are assigned as AuS stretching around 230 and 335 cm⁻¹. These values are lower than the corresponding frequencies assigned for complexes (1) and (2), which support the experimental trend and agree with the predicted structures where the Au-S bond length for complexes (2) and (4) were 2.38 and 2.40 Å, respectively.

NMR studies

In the ¹H NMR spectra, the hydrogen signals of the CH₂ and CH of the adamantane ligand appear in the δ 1.5–2.0 region. For ligand (A), a signal at δ 11.7 was also observed which was attributed to NH and disappears in the spectra of complexes (1) and (2). The calculated chemical shift for NH of ligand (A) was 8.0 ppm, which is in closer accordance with the experimental data than that predicted for the SH tautomer (4.9 ppm). These data support the predominance of the NH tautomer in solution, as previously assessed from thermodynamic data. The ¹H NMR spectra of ligand (B) show the signal of adamantane and three more signals: a singlet at δ 3.4 and two triplets at δ 3.2 and

Table 1 ^{13}C NMR chemical shift for the main atoms involved with the coordination to gold metal

	C2	C5	C6	C4
Ligand (A) ^a	178.5 (178)	170.6 (169)	–	–
(1)	176.2 (172)	160.3 (171)	–	–
(2)	174.6 (172)	168.5 (170)	–	–
Ligand (B) ^a	198.5 (199)	36.6 (35.6)	61 (62)	59.9 (61)
(3)	198.9 (201)	37.0 (37.5)	61.4 (66)	60.4 (64.9)
(4)	198.5 (201)	36.8 (37.1)	61.2 (65.5)	60.1 (64.5)

The values are in δ scale (ppm) relative to TMS. Calculated values are given in brackets (B3LYP/6-31 + G(2d,p)/SDD(f) level in CHCl_3 solution)

^a The atoms numbering is given in Schemes 1, 2

4.1 attributable to the CH_2 outside and inside the heterocyclic ring, respectively. For the complexes (1) and (3) signals were observed in the δ 7.2–7.7 region, corresponding to aromatic hydrogens of the PPh_3 group. For complexes (2) and (4) the signal attributed to CH_3 of PEt_3 group appears in the δ 1.1–1.3 region.

The ^{13}C NMR spectrum of the ligand (A) shows the signals of adamantane in the δ 26.7–40.9 region. The signal at δ 170.6 is attributed to the carbon directly bounded to the N and O in the heterocyclic ring (C5) and at δ 178.5 to the C(=S) (C2) (see Scheme 2 for numbering). These assignments are supported by theoretical calculations, which predicted the corresponding signals at δ 169 (C5) and 178 (C2). The chemical shifts for the carbon atoms in the adamantane moiety are calculated on the range of 35–44 ppm. For the ligand (B) the observed signals of adamantane were in the δ 27.4–41.3 region, and signals at δ 59.9 and δ 61.0 assigned to the CH_2 groups directly bound to the N3 (C4 and C6, respectively). The C(=S) (C2) signal is observed at δ 198.5. The theoretical ^{13}C NMR predictions for ligand (B) are in perfect accordance to the experimental assignments, with the main signals at δ 61 (CH_2 of the heterocyclic ring—C4), δ 62 (CH_2 connecting the adamantane to the heterocyclic ring—C6) and δ 199 (C=S—C2).

For the gold(I) complexes the ^{13}C NMR signals do not differ much from those predicted for the free ligands, except for the set of peaks due the phosphine ligand that were observed between 129 and 134 ppm to PPh_3 and 8–18 ppm to PEt_3 . Due to ^{13}C – ^{31}P coupling, the phenyl carbons of complexes (1) and (3) appear as doublets resonances as described in the literature [28]. The calculated spectra show the PPh_3 signals in the 125–135 ppm region and PEt_3 in the 8–25 ppm region for all four complexes, which is in accordance with the experimental data. The adamantane carbons are assigned to the 27–42 ppm region as predicted for the free ligand and supported by the theoretical spectra. For complexes (1) and (2), an upfield shift was observed for the signals corresponding to C2 (C=S) and C5 (C=N) 176/160 (1) and 174/168 ppm (2), respectively for C2 and C5 atoms. The calculated values follow the experimental trend: 172/171 ppm (1) and 172/170 ppm (2). Concerning complexes (3) and (4) the carbons C4, C6 and C2 (C=S) do not differ significantly from ligand (B). The ^{13}C NMR chemical shift and assignments are summarized in Table 1.

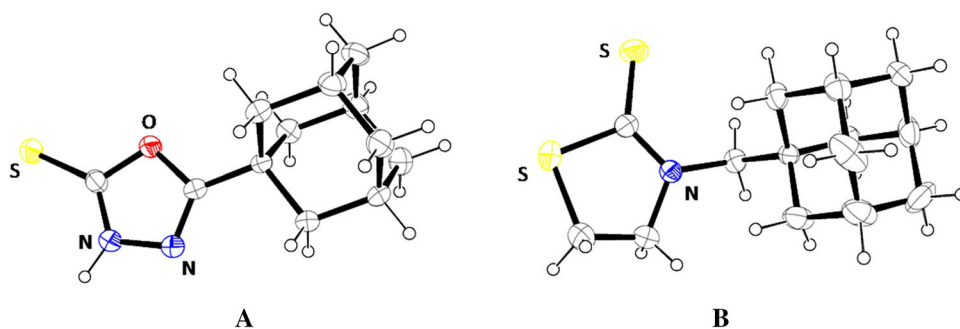
For the gold(I) complexes, the ^{31}P NMR spectrum presents a single resonance at δ 25.22 (1), 38.90 (2), 33.19 (3) and 33.43 (4) differing slightly from PPh_3AuCl (δ 33.17) and Et_3PAuCl (δ 33.45). In accordance to the other analysis, the complexes with oxadiazole derivative ligands (1 and 2) promote bigger interference in NMR signals than complexes with thiazoline derivative ligands (3 and 4).

In short, the Raman and NMR spectroscopic analyses, supported by DFT calculations, and mass spectroscopy, suggest the structures represented in Figs. 1, 2, 3, and 4. Some of them were confirmed by X-ray diffraction which was taken as a reference to assess the confidence limit of the molecular modeling studies. These are discussed in the next section.

X-ray structural determination

Crystals were obtained by recrystallization, from methanol for ligand (A), from ethanol for ligand (B) (Fig. 1) and

Fig. 1 ORTEP drawing of the crystal structures for ligand (a) and (b). The ellipsoids are drawn at the 50 % probability level and hydrogen atoms are shown as spheres of arbitrary radii



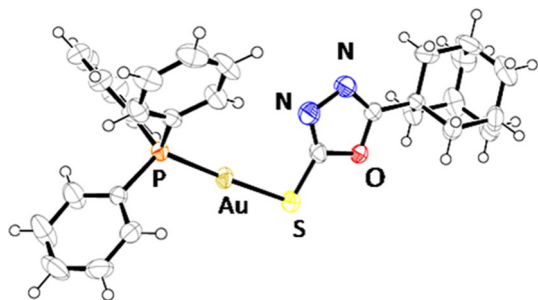


Fig. 2 ORTEP drawing of the crystal structures of complex (**1**). The ellipsoids are drawn at the 50 % probability level and hydrogen atoms are shown as spheres of arbitrary radii

from a mixture of dimethylsulfoxide and dichloromethane for complex (**1**), and isolated by filtration (Fig. 2). The structures were determined using single-crystal X-ray diffraction. Crystal data, data collection and structure refinement details are summarized in Table 2. Ligand (**A**) crystallizes in the monoclinic crystal system and $P2_1/c$ space group. Ligand (**B**) crystallizes in the monoclinic crystal system and $C2/c$ space group. The complex (**1**) crystallizes in the orthorhombic crystal system and $Pbca$ space group. Crystallographic analysis indicates that the asymmetric unit

of the complex (**1**) (Fig. 2) consists of one Au(I) ion, one PPh_3 molecule and one ligand (**A**). The Au(I) ion is coordinated by one P atom of the phosphine and one S atom of the ligand (**A**) in a slightly distorted linear geometry with coordination angle of $176.05(4)^\circ$. The asymmetric unit interacts with each other by non-classical hydrogen bonds of type C–H \cdots N (2.75 Å) and C–H \cdots O (2.64 Å), generating a three-dimensional arrangement as shown in Fig. 3 along the ac plane.

For ligands (**A**) and (**B**), the C2–S bond distances are 1.653(3) and 1.657(3) Å, respectively, which are shorter than the corresponding bonds in complex (**1**), C2–S = 1.715(4) Å. The predicted values for the C2–S bond length were 1.64 (A) and 1.65 Å (B), with bond order ~ 1.6 . For complex (**1**) the C2–S bond was 1.73 Å long with bond order ~ 1.2 . For complexes (**1**) and (**2**) two forms (s and a) were considered which differ by torsion around the C2–S bond. The conformer with the dihedral O1–C2–S–Au close to 180° (1-a and 2-a forms, Fig. 4) was the global minimum, favored by ~ 3.6 kcal mol $^{-1}$ regardless the phosphine ligand. This has been confirmed by X-ray diffraction for the complex (**1**), wherein the twist angle O1–C2–S–Au is $178.1(3)^\circ$. Some bond lengths and angles for complex (**1**) can be compared to the calculated values (in brackets):

Table 2 Crystal data of ligands (**A**) and (**B**) and complex (**1**)

Compound	Ligand (A)	Ligand (B)	Complex (1)
Formula	C ₁₂ H ₁₆ N ₂ OS	C ₁₄ H ₂₁ NS ₂	C ₃₀ H ₃₀ AuN ₂ OPS
Formula weight/g mol $^{-1}$	236.33	267.44	694.56
Temperature/K	298 (2)	298(2)	298(2)
Crystal system	Monoclinic	Monoclinic	Orthorhombic
Space group	$P2_1/c$	$C2/c$	$Pbca$
$a/\text{Å}$	10.5545 (16)	25.225 (2)	19.3397 (5)
$b/\text{Å}$	11.0918 (14)	9.9815 (6)	10.5189 (3)
$c/\text{Å}$	10.2864 (17)	10.8885 (8)	26.2493 (8)
$\alpha/^\circ$	90.00	90	90
$\beta/^\circ$	100.330 (14)	98.063 (7)	90
$\gamma/^\circ$	90.00	90	90
$V/\text{Å}^3$	1184.69 (31)	2714.4 (3)	5240.0 (3)
Z	4	8	8
Crystal size/mm	0.85 × 0.38 × 0.28	0.41 × 0.14 × 0.08	0.31 × 0.13 × 0.11
$D_{\text{calc}}/\text{g cm}^{-3}$	1.325	1.309	1.728
$\mu(\text{Mo K}\alpha)/\text{cm}^{-1}$	0.254	0.371	5.675
Transmission factors (min/max)	0.886/0.944	0.936/0.981	0.989/0.995
Reflections measured/unique	5322/2411	13870/2776	38442/5463
Observed reflections	1573	2083	4024
N $^\circ$. of parameters refined	149	214	326
$R[F_o > 2\sigma(F_o)]$	0.053	0.054	0.029
$wR[F_o, 2 > 2\sigma(F_o)^2]$	0.152	0.136	0.048
S	1.002	1.033	1.060
RMS peak/	0.095	0.064	0.093

Fig. 3 View of the molecular packing diagram along *ac* plane

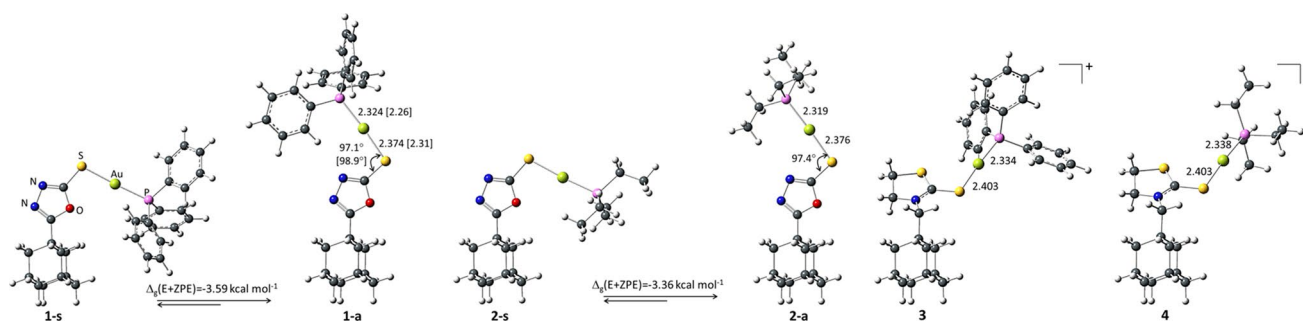
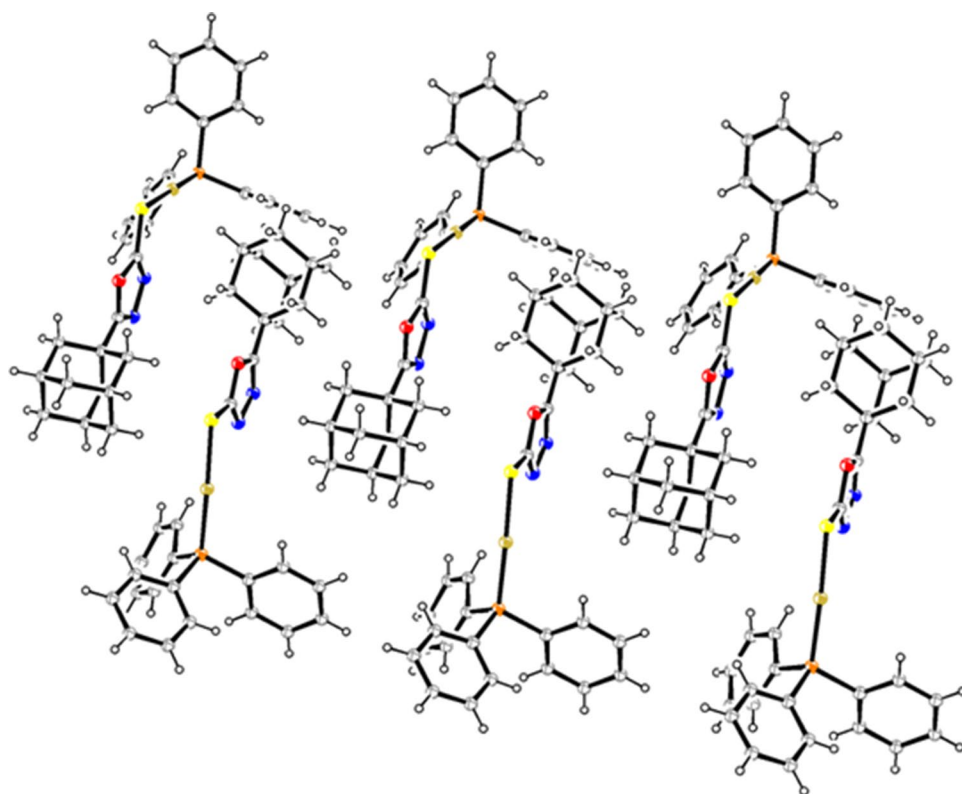


Fig. 4 Calculated geometries for the gold(I) complexes (gas phase at B3LYP/6-31+G(2d)/SDD(f) level). For complexes (1) and (2), two distinct conformer are shown (“s” and “a”), differing by the relative

position around the C2–S bond (the relative energy including ZPE correction is also provided). Some bond lengths and angle are shown with experimental values in brackets

Au–S–C2 = 98.88(13)° [97.1°]; S–Au = 2.3122(11) Å [2.374 Å] and Au–P = 2.2584(11) Å [2.324 Å]. The S–Au–P angle was 176° in the solid state and in gas phase, suggesting that the intermolecular forces do not change significantly the geometry of complex (1) around the coordination sphere. Similar geometry is predicted for complex (2) as seen in Fig. 4. Interestingly, for the analogue complex containing the 5-phenyl-1,3,4-oxadiazole-2-thione ligand (complex 4 in Ref. [28]), the X-ray structure was assigned as the form “s” (similar to 2-s in Fig. 4) with O1–C2–S–Au torsion angle of 13.60°. This finding was mainly due to weak unconventional C–H⋯N hydrogen

bonds (distance ~2.7 Å), which lead to the formation of a two-dimensional array in solid state and, therefore, stabilizing the overall structure.

For complexes (3) and (4) only one conformer was considered as represented in Fig. 4. The coordination through S1 (see Schemes 1, 2 for numbering sequence) was also considered, but the resulting structure was 15 kcal mol⁻¹ higher in energy (not shown). The C2–S bond length for complexes (3) and (4) was 1.71 Å, slightly shorter than the corresponding bonds in (1) and (2), with bond order ~1.3. The N3–C2–S–Au dihedral was around 171° and the C2–S–Au angle close to 107°. As expected, the ligand

Table 3 Cytotoxic activities against cell lines, inhibition activity of TrxR and GSH interaction

Compounds	Tumor cells IC ₅₀ ($\mu\text{M} \pm \text{SD}$) ^a						Non-tumor cells BHK21	TrxR Inhibition (% \pm SD)	GSH Interaction (% \pm SD)
	B16-F10	SI ^b	CT26-WT	SI ^b	4T1	SI ^b			
A	>100	ND	55.0 \pm 17	ND	>100	ND	>100	51.7 \pm 2.1 ^c	<0.1
1	5.7 \pm 0.5	3.2	5.7 \pm 0.9	3.2	6.6 \pm 0.5	2.8	18.5 \pm 2.9	40.7 \pm 1.5 ^c	21.1 \pm 2.0
2	1.2 \pm 0.2	4.5	1.8 \pm 0.8	3.0	1.6 \pm 0.5	3.4	5.5 \pm 0.1	51.6 \pm 1.6 ^c	33.3 \pm 1.0
B	9.0 \pm 0.6	1.9	34.2 \pm 0.9	0.5	30.9 \pm 3.2	0.5	17.2 \pm 6.7	35.7 \pm 2.2 ^c	<0.1
3	1.8 \pm 0.5	3.8	1.8 \pm 0.3	3.8	3.0 \pm 1.8	2.3	6.9 \pm 0.8	57.3 \pm 0.7 ^c	11.0 \pm 4.1
4	1.0 \pm 0.1	5.8	0.9 \pm 0.1	6.4	1.1 \pm 0.2	5.3	5.8 \pm 0.1	60.2 \pm 0.7 ^c 32.0 \pm 1.7 ^d 27.0 \pm 0.5 ^e	51.2 \pm 1.5
AuPPh ₃ Cl	6.6 \pm 0.1	3.4	12.1 \pm 2.8	1.9	10.3 \pm 2.3	2.2	23.0 \pm 0.3	–	14.9 \pm 3.2
AuPEt ₃ Cl	2.3 \pm 0.5	9.7	9.0 \pm 0.7	2.5	9.5 \pm 1.1	2.4	22.5 \pm 0.2	–	52.0 \pm 2.0
Auranofin	0.5 \pm 0.4	3.2	0.5 \pm 0.4	3.2	0.6 \pm 0.2	2.7	1.6 \pm 0.5	59.7 \pm 1.5 ^c 61.9 \pm 2.0 ^d 59.7 \pm 1.5 ^e	16.5 \pm 1.0
Cisplatin	6.0 \pm 1.0	3.0	5.0 \pm 1.7	3.6	6.2 \pm 2.5	2.9	18.1 \pm 10.9	–	–

^a SD standard deviation of quadruplicate of two independent experiments

^b SI selectivity index– the ratio of the IC₅₀ obtained from the experiment on normal cells vs. tumor cells

^c Concentration of compounds in TrxR assay (5 μM)

^d Concentration of compounds in TrxR assay (1 μM)

^e Concentration of compounds in TrxR assay (0.5 μM)

ND not determined

arrange in a linear geometry around the gold center, with $\angle\text{S–Au–P} = 176^\circ$ for all complexes.

Biological tests

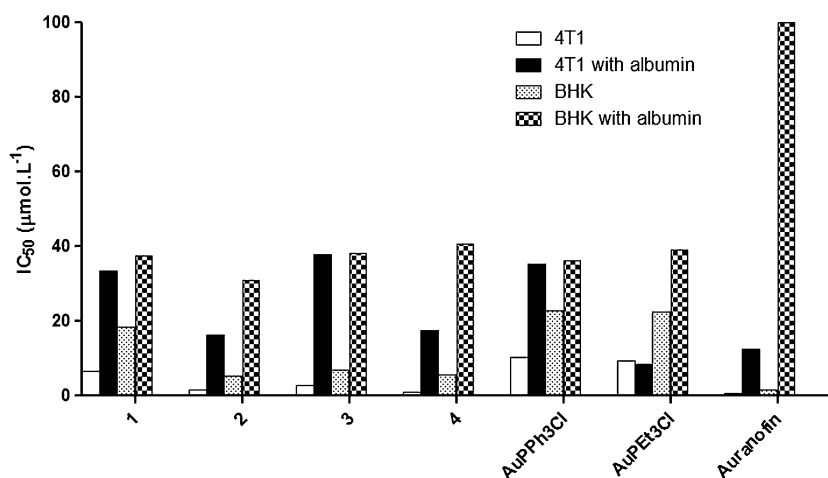
The cytotoxic activity of the compounds was evaluated in comparison with auranofin and cisplatin in three tumor cell lines to assess the activity in different embryonic origin (epithelial and fibroblast) and also in a normal kidney cell that was used to evaluate the selectivity index. IC₅₀ values, calculated from the cell viability dose response curves obtained after 72 h drug treatment in the MTT test and percentage of inhibition of TrxR are shown in Table 3.

All gold complexes were more active in the tested cell lines than their respective ligands and phosphane gold precursor complexes [Et₃PAuCl] and [Ph₃PAuCl] presenting higher selectivity in most of the cases. In general, oxadiazole complexes were up to 80 times more active than the free ligand whereas thiazolidine complexes were up to 38 times more active than the free ligand. The thiazolidine complexes were more active than oxadiazole complexes in all cases. These results can be explained in part by the activity presented by the free ligand. Comparing different phosphine ligands, complexes with triethylphosphine (**2**) and (**4**) were more active than their triphenylphosphine analogues (**1**) and (**3**), which is reflected in the same profile presented by [Et₃PAuCl] and [Ph₃PAuCl] (Table 3). We

noticed that the presence of adamantyl-heterocyclic ligand improved cytotoxicity and justifies the designing new ligands for Au(I) complexes. All complexes were more efficient and selective than cisplatin to murine melanoma cell line (B16-F10). With respect to CT26-WT (murine colon carcinoma), the complexes (**3**) and (**4**) were more active (IC₅₀ = 1.8 \pm 0.3 μM and IC₅₀ = 0.9 \pm 0.1 μM , respectively) than cisplatin (IC₅₀ = 5.0 \pm 1.7 μM). In metastatic mouse mammary adenocarcinoma (4T1) the complexes with triethylphosphine (**2**) (IC₅₀ = 1.6 \pm 0.5 μM) and (**4**) (IC₅₀ = 1.1 \pm 0.2 μM) present better results when compared to cisplatin (IC₅₀ = 6.2 \pm 2.5 μM), even for selectivity. Complex (**4**) showed IC₅₀ values close to the auranofin; however, it has a greater SI for the tested cell lines that presents a combination of alkyl phosphine and thiazolidine ligands.

We also observed the effect of albumin upon cytotoxicity of the compounds. Albumin has one free cysteine residue that can promote sulfhydryl exchange reactions. In cells exposed concomitantly to albumin and gold compounds, the IC₅₀ obtained showed a protective effect of albumin increasing values up to ten times in tumor cells (4T1) and up to five times in normal cells (BHK-21). These results are showed in Fig. 5 and suggest the metabolic role of albumin in gold complexes that was previously reported for gold anti-arthritis drugs. More than 80 % of the circulation gold in treated patients is bound to plasma protein

Fig. 5 Effect of albumin in cytotoxic activities against tumor cell line 4T1 and normal cell line BHK-21



albumin [41]. From structure–activity analyses, we noticed that the triethylphosphine derivatives remain more active than the triphenylphosphine analogues even in presence of albumin.

The assays of inhibition of TrxR can be related with cytotoxicity, except for ligand (A) that even inhibited TrxR but did not show any activity in analyzed cells. The difference may be explained by transport into the cell. The results show values between 36 and 60 % of enzymatic inhibition. The triethylphosphine complexes are slightly more active than the triphenylphosphine analogues, and thiazolidine are more potent than the oxadiazole analogues. [Et₃PAuCl] and [Ph₃PAuCl] are well known as TrxR inhibitors and this has been previously discussed in the literature [55]. Complex (4), the most cytotoxic complex, also showed the best inhibition when compared to auranofin. Auranofin showed higher inhibition effect even at 0.5 and 1.0 µM (58 %) concentration levels, which complex (4) inhibit 27 and 32 %, respectively, reaching the same Auranofin inhibition activity only at 5 µM, Fig. 6.

respectively, reaching the same Auranofin inhibition activity only at 5 µM, Fig. 6.

Glutathione is another –SH target for gold drugs. The results in Table 3 show, as expected, no significant interaction for ligands and different potential interaction with gold compounds. An interesting structure–reactivity relationship is observed where the triethylphosphine analogues (2,4) are more susceptible for reaction with glutathione, which are in line with the TrxR inhibition.

Different sulfur targets can interact with gold drugs as it is already knew for auranofin and, therefore, some competition can occur protecting cells from their action, but these interactions are not able to deactivate 100 % of the drug that still is active in tumor cells.

DFT and docking analyses of the ligand-TrxR binding

Molecular modeling analyses including DFT calculations and drug-receptor docking were conducted in the present study aiming to gain some insights into the binding modes of the novels TrxR inhibitors described herein. It is well accepted that the C-terminal moiety of TrxR (–G496–C497–U498–G499–) is the main target for gold-containing inhibitors due to the very attractive soft base Sec-498 residue [55]. Firstly, the ligand exchange reactions for complexes (1–4) were investigated where the ligands (A) or (B) were taken as the leaving groups and the Sec amino acid as the entering group. The sulfur ligand is more likely to be replaced due to the high *trans* effect of the phosphine moiety. An associative mechanism, with the proton transfer observed upon nucleophilic attack, was assumed as described previously for auranofin [46] where a distorted trigonal planar geometry is proposed for the transitions state (TS). The reactive species for the direct reactions, including the TS structures, are represented in Fig. 7. The structural parameters around the first coordination sphere are also shown in addition to the Gibbs free energy

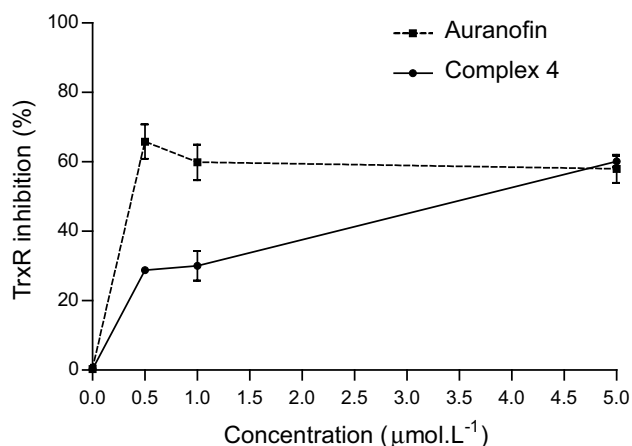


Fig. 6 Inhibition of TrxR activity by Auranofin and Complex 4 in different concentrations (0.5, 1.0, 5.0 µM). Experiments were performed in triplicate and the results represent the mean ± SD

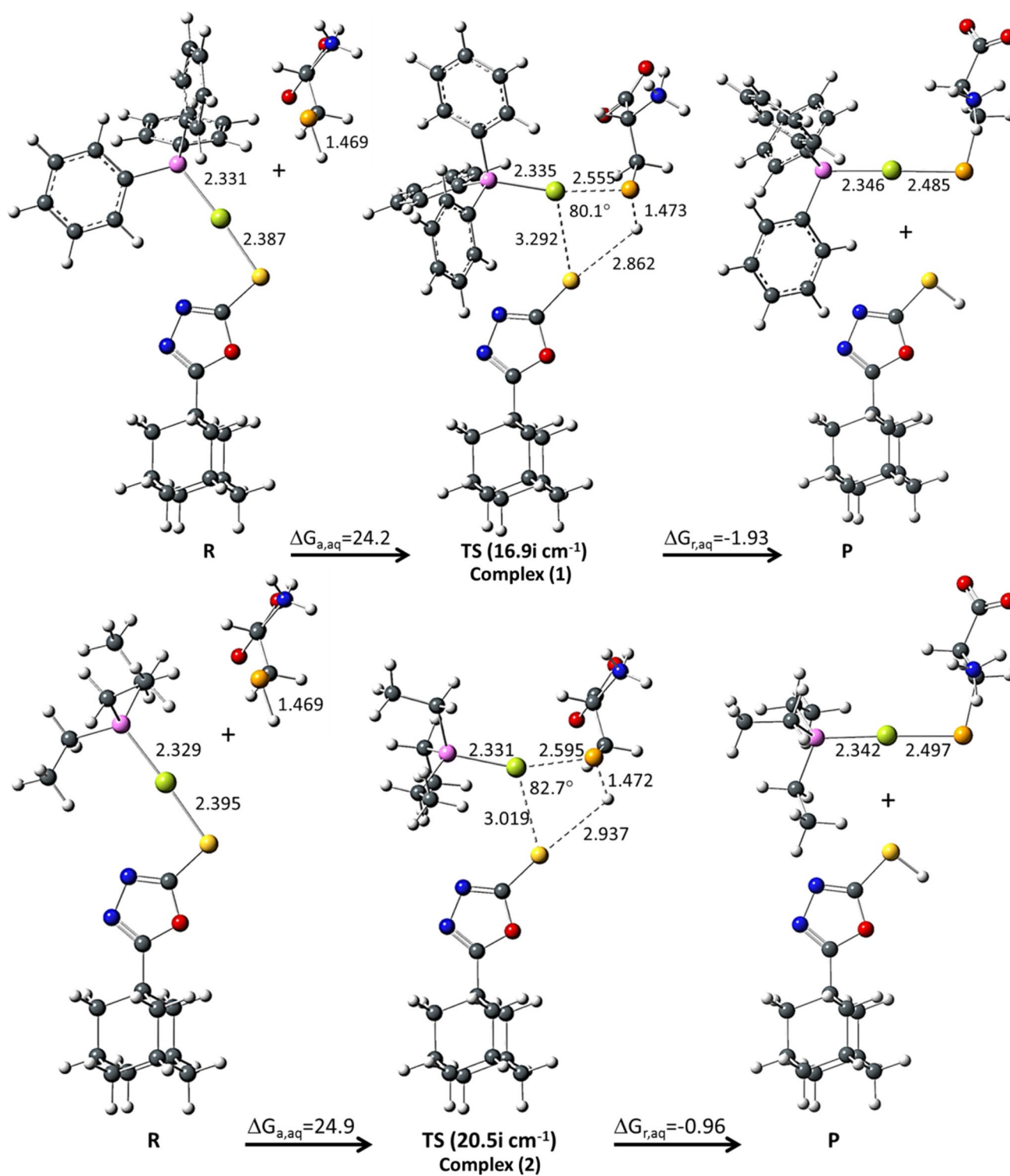


Fig. 7 Reagents (R), transition states (TS) and products (P) calculated for the ligand exchange reactions of the gold complexes. The structures were optimized in aqueous solution at B3LYP/6-

31+G(2d)/SDD(f). The free energy barrier ($\Delta G_{a, aq}$) and reaction free energy ($\Delta G_{r, aq}$) are in kcal mol⁻¹ and bond lengths in Å

barrier ($\Delta G_{a, aq}$) and reaction Gibbs free energy ($\Delta G_{r, aq}$). The structures and energies were calculated at B3LYP/6-31+G(2d)/SDD(f) level in aqueous solution.

It is well accepted that ligand exchange rate might be relevant for the final biological response of metal-based drugs. In our previous study, a structure–activity relationship

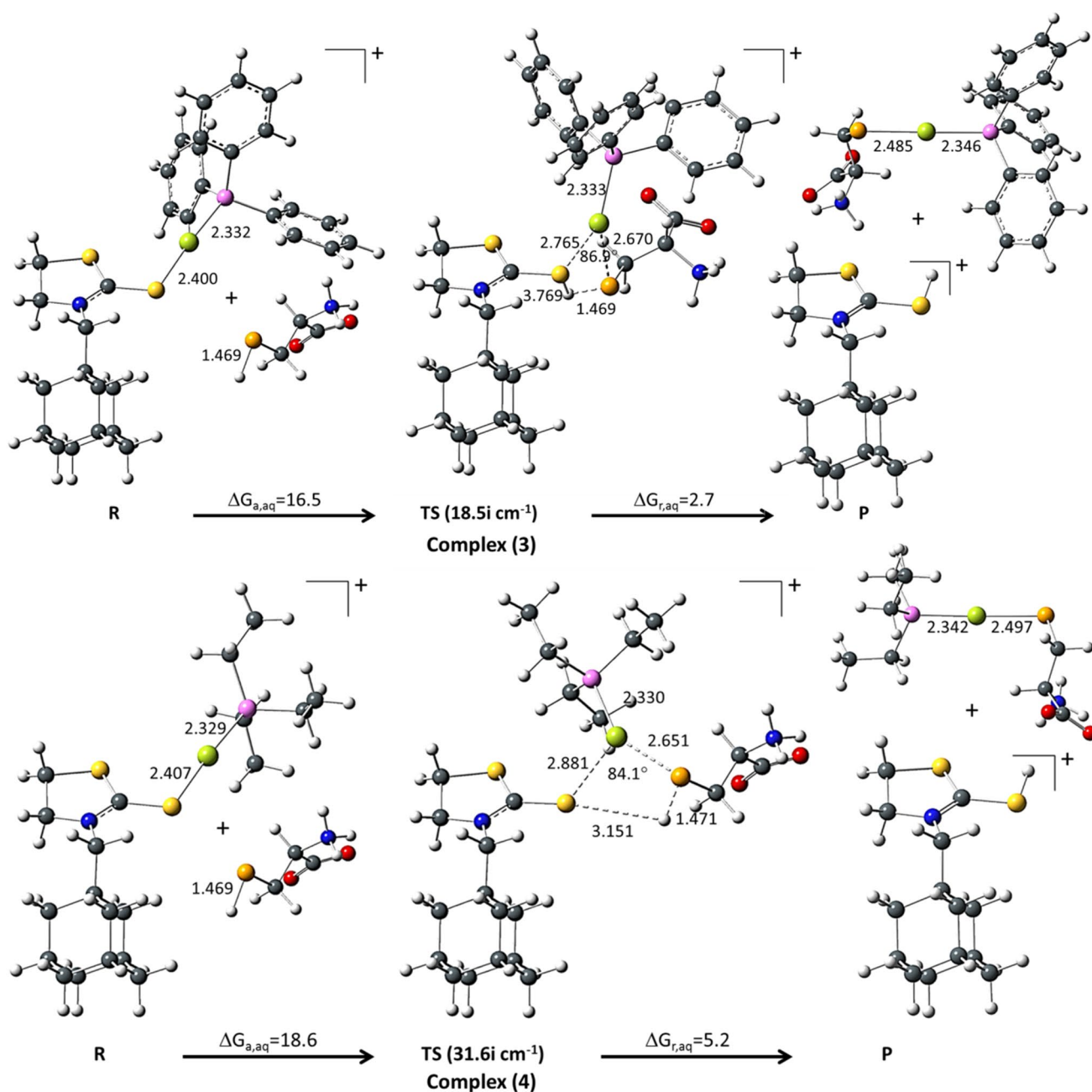


Fig. 7 continued

(SAR) was established for a series of Pt(II) complexes using mutagenicity and the hydrolysis rate constants as dependent and independent variables, respectively [56]. From Fig. 7, it is evident that the ligand-exchange reactions for thiazolidine complexes (3) and (4) are much faster (lower energy barrier— $\Delta G_{a, aq} \sim 17$ kcal mol⁻¹) than for oxadiazoline complexes (1) and (2) ($\Delta G_{a, aq} \sim 24$ kcal mol⁻¹), even though the processes for the latter are slightly more favorable. The reactivity of these complexes using water as nucleophile was also theoretically predicted and the same trend

as that found for Sec nucleophilic attack could be established, the hydrolysis process being slower than the attack of the Sec amino acid (data not shown). To illustrate, for complex (2) the reaction with Sec residue was four times faster than the reaction with water, whereas for complex (4) the rate ratio was almost three orders of magnitude greater. Moreover, it might be concluded based on solid theoretical grounds that although complexes (3) and (4) react quickly with the Sec residue, they are relatively stable in aqueous solution. The same is true for oxadiazoline complexes (1)

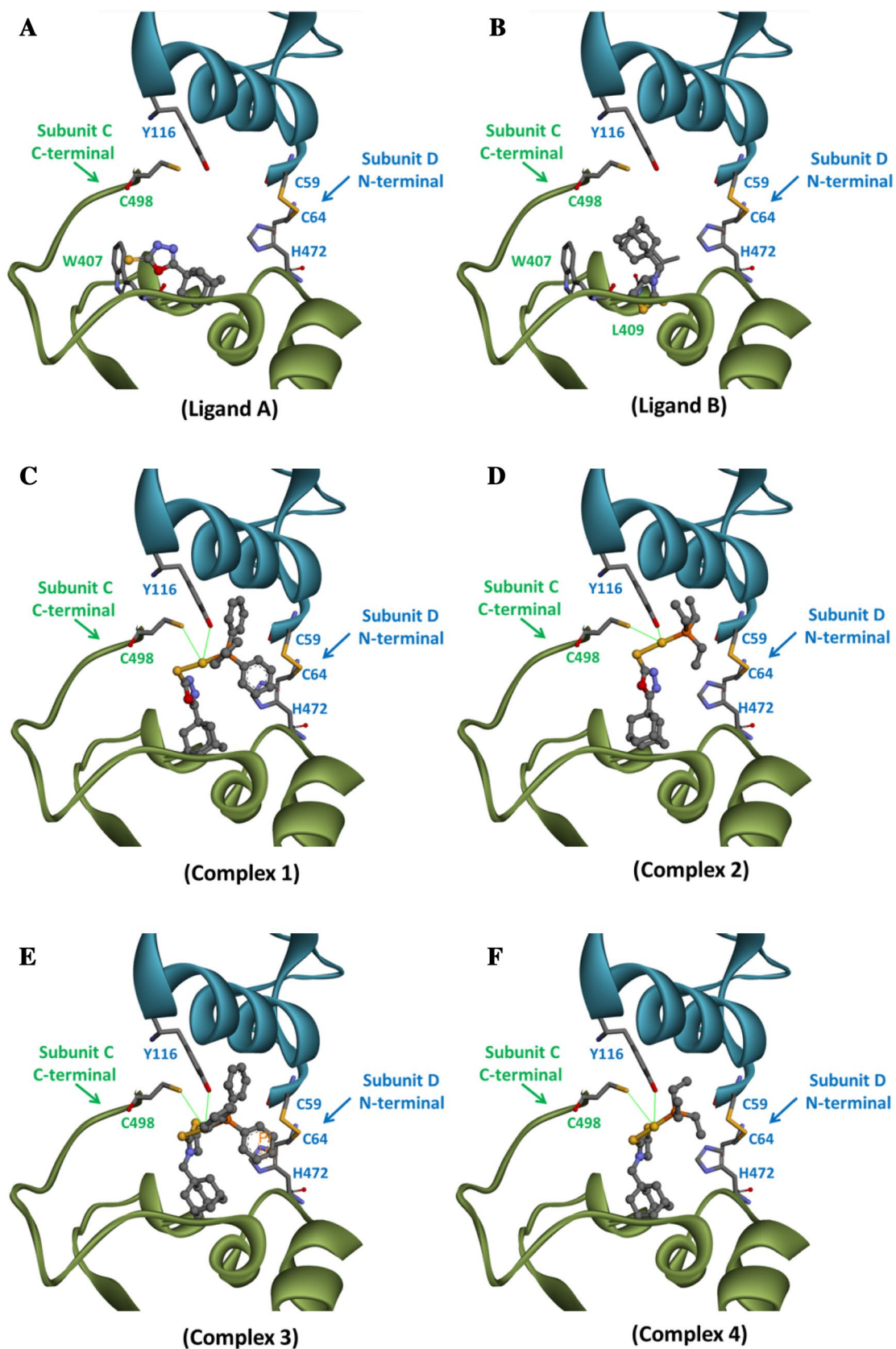


Fig. 8 Scheme of the TrxR binding site composed by Subunits C (C-terminal motif) and D (N-terminal motif). The ligand-receptor binding modes for the compounds studied, as predicted from docking analysis, are shown

and (2). The reaction of auranofin with Sec was described previously [46] using the very same level of theory applied here. The results were (in kcal mol⁻¹) $\Delta G_{a, \text{aq}} = 29.8$ and $\Delta G_{r, \text{aq}} = -5.5$, which are closer to those found for oxadiazoline derivatives (see Fig. 7). For analogue compounds, the kinetic parameters might be related with biological responses as shown for platinum complexes [56]. From Fig. 7 and Table 3 we note that the most reactive complexes (3) and (4) show higher cytotoxicity and higher enzyme inhibition compared to the corresponding (1) and (2) oxadiazoline derivatives, which is evidence that the rate of ligand exchange might play a role on drug–enzyme binding and thereby contribute to the overall biological response. The structure–reactivity relationship proposed previously [45, 46] is also observed here, with the energy barrier decreasing with an increase of the “reactive angle” between the entering and leaving groups (see angles values in Fig. 7).

Lastly, the ligand–receptor docking analysis was performed for the free ligands and gold(I) complexes. The best *pose* for each compound (highest score) is represented in Fig. 8 with the main amino acid residues defining the binding pocket also included. Only one of the two active sites in dimeric TrxR enzyme is represented, which is located at the interface between the Subunits C (C-terminal motif –G496–C497–C498–G499–) and D (N-terminal motif –C59–V60–N61–V62–G63–C64–). For the free ligands (Fig. 8a, b) the binding modes involve one hydrogen bond in addition to several hydrophobic contacts. For ligand (A) a relatively strong hydrogen bond is predicted with residue W407, which acts as a hydrogen donor. The N–H...O1 distance was 1.84 Å. For ligand (B), a weak hydrogen bond is also observed involving the residue L409, with the N–H...S=C hydrogen bond distance equal to 2.03 Å. It is noteworthy that for such small molecules where specific anchoring points are not found, the prediction of the best *pose* is a challenge. Nonetheless, the strong hydrogen bond predicted for ligand (A) might provide additional evidence for the higher biological response of ligand (A) compared to ligand (B) when TrxR inhibition is considered, even though, it was not observed in cytotoxicity studies (see Table 3). When considering gold(I) complexes, the hydrophobic interactions dominate and the best binding *poses* predicted are similar for all complexes (Fig. 8c, d, e, f). The adamantane ring lies over the Subunit C which acts as a hydrophobic cushion, and the phosphine ligand is pointed towards the N-terminal motif. Both ligands are involved in van der Waals contacts, with electrostatic interaction observed only between the metal center and C498 and Y116 residues. It is important to bear in mind that these docking runs were conducted under Au–S(C498) distance constraint, therefore the C498–Au short contact is not meaningful and was used as a bouldering condition to set up the gold complex close to the enzyme reactive center.

Nonetheless, the Au–S(C498) distances were around 3.6 and 4.0 Å for oxadiazoline and thiazolidine complexes, respectively, which are in line with the corresponding distances calculated for the TS structures shown in Fig. 7. For the complexes (1) and (3) an additional π -stacking interaction is predicted involving the phenyl ring from P(Ph)₃ ligand and H472 residue.

For all complexes analyzed, the docked structure assumes a “folded” form, in between the “s” and “a” conformers, with the torsion angle around the C–S bond $\sim 85^\circ$ – 130° in the enzyme complex compared to $\sim 171^\circ$ – 180° in the isolated complex. This finding suggests that this “folded” form fits better to the TrxR binding site and thus puts the complex in a more favorable position for nucleophilic attack, which is an important event to improve TrxR inhibition. For complexes (2) and (4) (Fig. 8d, e, f), the strongest TrxR inhibitors according Table 3, the PLP score was 52 and 57, which is in line with observed biological responses quoted in Table 3.

From previous analyses, we may suggest some molecular features for the mechanism of action for the compounds reported herein considering TrxR as the primary target: (1) the compounds prepared should interact in a competitive mode with the thioredoxin (trx) binding site, namely the pocket around the C-terminal motif of TrxR enzyme; (2) no specific anchoring points are observed over the docking mode, with ligand (A) being the only compound showing a moderate hydrogen bond with the W407 residue, remembering that ligand (A) is more potent as an enzyme inhibitor than ligand (B); (3) for all four gold complexes the docking modes are driven by hydrophobic interaction; (4) As generally accepted for metallodrugs, the chelating ability is the main feature responsible for the biological response. For the described gold complexes, the best biological response (TrxR inhibition) was observed for complexes (3) and (4), which were fairly reactive with the Sec residue; (5) A “folded” form in between the “s” and “a” conformers of the complexes seems to play a role in the docking mode.

Concluding remarks

The present work describes the synthesis and characterization of two ligands and four novel gold(I) complexes considered as potential anticancer drugs. The structural characterization of the compounds was established on the basis of elemental analysis and spectroscopic data with the aid of DFT calculations. For complex (1), the X-ray structure was obtained and used as reference to propose the structures of the other complexes and assess the theoretical protocol. Complex (4) was shown to be more selective than auranofin and quite similar in cytotoxicity. Moreover, albumin interference, glutathione interaction and TrxR inhibition was

tested and correlated with assays in tumor cells. Even for gold complexes interacting to other thiol containing molecules, the results suggest TrxR as possible target for these compounds. Complex (**4**) with triethylphosphine and thiazolidine ring was the most cytotoxic and active against TrxR among the tested analogues.

Molecular modeling was investigated in order to obtain insights on the mechanism of action. The first approach was to evaluate the reactivity of the gold complexes against the Sec residue. The results showed that the most active complexes (**3,4**) react with Sec much faster than complexes (**1,2**). The rate constant for the ligand exchange process was in the order of $10 \text{ M}^{-1} \text{ s}^{-1}$ for complexes (**3,4**) and $10^{-5} \text{ M}^{-1} \text{ s}^{-1}$ for complexes (**1,2**). Therefore, the higher biological response for complexes (**3,4**) might be due to the faster ligand exchange upon interaction with the TrxR binding site. In the second approach, molecular docking was accomplished for both free ligands and all gold complexes. Concerning the free ligands, the best TrxR inhibitor was observed to be ligand (**A**), which showed a short hydrogen bond (1.84 \AA) with the W407 residue. For ligand (**B**) and all gold complexes, the hydrophobic contacts dominate, with the adamantane ligand playing a role for ligand-receptor stabilization. Interestingly, for all complexes a conformation change is predicted from “a” to a “folded” form, characterized by a torsion around the C–S bond. Even though we do not have a causative relationship, the “folded” form might serve as template to design molecules with potential for inhibiting the TrxR enzyme.

Acknowledgments The authors wish to thank CNPq, FAPEMIG and CAPES for financial supports and fellowships. HFDS would like to thank CNPq (485779/2013-7) and HS (455548/2014-5) for providing support for this study. This work is a collaborative research project with members of Rede Mineira de Química (RQ-MG) supported by FAPEMIG (Project: CEX - RED-0010-14) and HS (APQ-01648-14).

References

- Sutton BM (1986) *Gold Bull* 19:15–16
- Forestier J (1934) *The Lancet* 646–648
- Berners-Price SJ, Filipovska A (2011) *Metalomics* 3:863–873
- Madeira JM, Gibson DL, Kean WF, Klegeris A (2012) *Inflammopharmacology* 20:297–306
- Gandin V, Fernandes AP, Rigobello MP, Dani B, Sorrentino F, Tisato F, Bjornstedt M, Bindoli A, Sturaro A, Rella R, Marzano C (2010) *Biochem Pharmacol* 79:90–101
- Rubbiani R, Schuh E, Meyer A, Lemke J, Wimberg J, Metzler-Nolte N, Meyer F, Mohr F, Ott I (2013) *Med Chem Commun* 4:942–948
- Messori L, Marchetti L, Massai L, Scaletti L, Guerri A, Landini I, Nobili S, Perrone G, Mini E, Leoni P, Pasquali M, Gabbiani C (2014) *Inorg Chem* 53:2396–2403
- Rigobello MP, Folda A, Dani B, Menabo R, Scutari G, Bindoli A (2008) *Eur J Pharmacol* 582:26–34
- Marzano C, Gandin V, Folda A, Scutari G, Bindoli A, Rigobello MP (2007) *Free Radical Biol Med* 42:872–881
- Messori L, Scaletti F, Massai L, Cinellu MA, Gabbiani C, Vergara A, Merlino A (2013) *Chem Commun* 49:10100–10102
- Liu C, Liu Z, Li M, Li X, Wong Y-S, Ngai S-M, Zheng W, Zhang Y, Chen T (2013) *Plos One* 8:e53945
- Ortego L, Cardoso F, Martins S, Fillat MF, Laguna A, Meireles M, Villacampa MD, Gimeno MC (2014) *J Inorg Biochem* 130:32–37
- Rubbiani R, Kitanovic I, Alborzinia H, Can S, Kitanovic A, Onambele LA, Stefanopoulou M, Geldmacher Y, Sheldrick WS, Wolber G, Prokop A, Woelfl S, Ott I (2010) *J Med Chem* 53:8608–8618
- Meyer A, Gutierrez A, Ott I, Rodriguez L (2013) *Inorg Chimica Acta* 398:72–76
- Liu N, Huang H, Dou QP, Liu J (2015) *Oncoscience* 5:457–466
- Garcia-Moreno E, Gascon S, Atrian-Blasco E, Rodriguez-Yoldi MJ, Cerrada E, Laguna M (2014) *Eur. J Med Chem* 79:164–172
- Lessa JA, Guerra JC, de Miranda LF, Romeiro CFD, Da Silva JG, Mendes IC, Speziali NL, Souza-Fagundes EM, Beraldo H (2011) *J Inorg Biochem* 105:1729–1739
- Meyer A, Oehninger L, Geldmacher Y, Alborzinia H, Wolf S, Sheldrick WS, Ott I (2014) *ChemMedChem* 9:1794–1800
- Sun SY, Yue P, Hong WK, Lotan R (2000) *Cancer Res* 60:7149–7155
- Horvat M, Uzelac L, Marjanovic M, Cindro N, Frankovic O, Mlinaric-Majerski K, Kralj M, Basaric N (2012) *Chem Biol Drug Des* 79:497–506
- Parkes JD, Baxter RC, Marsden CD, Rees JE (1974) *J Neurol Neurosurg Psychiatr* 37:422–426
- Bleich S, Wiltfang J, Kornhuber J (2003) *N Engl J Med* 349:609–610
- Manjunatha K, Poojary B, Lobo PL, Fernandes J, Kumari NS (2010) *Eur J Med Chem* 45:5225–5233
- Kadi AA, El-Brollosy NR, Al-Deeb OA, Habib EE, Ibrahim TM, El-Emam AA (2007) *Eur J Med Chem* 42:235–242
- Kadi AA, Al-Abdullah ES, Shehata IA, Habib EE, Ibrahim TM, El-Emam AA (2010) *Eur J Med Chem* 45:5006–5011
- Bektas H, Ceylan S, Demirbas N, Alpay-Karaoglu S, Sokmen BB (2013) *Med Chem Res* 22:3629–3639
- Patel MB, Modi NR, Raval JP, Menon SK (2012) *Org Biomol Chem* 10:1785–1794
- Chaves JDS, Neumann F, Francisco TM, Corrêa CC, Lopes MTP, Silva H, Fontes APS, De Almeida MV (2014) *Inorg Chimica Acta* 414:85–90
- Serebryanskaya TV, Lyakhov AS, Ivashkevich LS, Schur J, Frias C, Prokop A, Ott I (2015) *Dalton Trans* 44:1161–1169
- Silva H, Barra CV, Costa CF, Almeida MV, César ET, Silveira JN, Paula FCS, Maia ECP, Fontes APS (2008) *J Inorg Biochem* 102:767–772
- Scheffler H, You Y, Ott I (2010) *Polyhedron* 29:66–69
- V. 1.171.35.21 (release 17–11–2008 Oxford Diffraction Ltd., 13:58:09) *CrysAlis171. NET*
- Sheldrick GM (2008) *Acta Cryst A* 64:112–122
- Byrnes MJ, Chisholm MH, Clark RJH, Gallucci JC, Hadad CM, Patmore NJ (2004) *Inorg Chem* 43:6334–6344
- Sun YG, Jiang B, Cui TF, Xiong G, Smet PF, Ding F, Gao EJ, Lv TY, Van den Eeckhout K, Poelman D, Verpoort F (2011) *Dalton Trans* 40:11581–11590
- Blessing RH (1995) *Acta Crystallogr Sect A* 51:33–38
- Farrugia LJ (1997) *J Appl Crystallogr* 30:565
- Al-Deeb A, Al-Omar MA, El-Brollosy NR, Habib EE, Ibrahim TM, El-Emam AA (2006) *Arzneim Forsch Drug Res* 56:40–47
- Sullivan FAV, Lindaw AC (1965) U.S. Patent 3.215.703
- Baenziger NC, Bennet WE, Soboroff DM (1976) *Acta Crystallogr Sect B* 32(3):962–963

41. Garcia-Orad A, Arizti P, Sommer F, Silvestro L, Massiot P, Chevallier P, Gutierrez-Zorrilla JM, Martinez de Pacorbo M, Colacio E, Tapiero H (1993) *Biomed Pharmacother* 47:363–370
42. Becke AD (1993) *J Chem Phys* 98:5648–5652
43. Andrae D, Haussermann U, Dolg M, Stoll H, Preuss H (1990) *Theor Chim Acta* 77:123–141
44. Dos Santos HF, Paschoal D, Burda JV (2012) *Chem Phys Lett* 548:64–70
45. Dos Santos HF, Paschoal D, Burda JV (2012) *J Phys Chem A* 116:11015–11024
46. Dos Santos HF (2014) *Comput Theor Chem* 1048:95–101
47. Scalmani G, Frisch MJ (2010) *J Chem Phys* 132:114110
48. Frisch MJ et al. (2009) Gaussian 09, Revision A.02, Gaussian Inc, Wallingford CT
49. Jones G, Willett P, Glen RC (1995) *J Mol Biol* 245:43–53
50. Jones G, Willett P, Glen RC, Leach AR, Taylor R (1997) *J Mol Biol* 267:727–748
51. Verdonk ML, Cole JC, Hartshorn MJ, Murray CW, Taylor RD (2003) *Proteins Struct Funct Genet* 52:609–623
52. Fritz-Wolf K, Urig S, Becker K (2007) *J Mol Biol* 370:116–127
53. Discovery Studio v3.5.0.12158. (2005) Accelrys Inc
54. Rao CNR, Venkataraghavan R (1962) *Spectrochim Acta* 18:541–547
55. Bindoli A, Rigobello MP, Scutari G, Gabbiani C, Casini A, Messori L (2009) *Coord Chem Rev* 253:1692–1707
56. Costa LAS, Rocha WR, De Almeida WB, Dos Santos HF (2005) *J Inorg Biochem* 99:575–583